

CRACK PATH SELECTION IN ADHESIVELY BONDED JOINTS

Buo Chen

(ABSTRACT)

This dissertation is to obtain an overall understanding of the crack path selection in adhesively bonded joints. Using Dow Chemical epoxy resin DER 331[®] with various levels of rubber concentration as an adhesive, and aluminum 6061-T6 alloy with different surface pretreatments as the adherends, both symmetric and asymmetric double cantilever beam (DCB) specimens are prepared and tested under mixed mode fracture conditions in this study. Post-failure analyses conducted on the failure surfaces indicate that the failure tends to be more interfacial as the mode II component in the fracture increases whereas more advanced surface preparation techniques can prevent failure at the interface. Through mechanically stretching the DCB specimens uniaxially until the adherends are plastically deformed, various levels of T-stress are achieved in the specimens. Test results of the specimens with various T-stresses demonstrate that the directional stability of cracks in adhesive bonds depends on the T-stress level. Cracks tend to be directionally stable when the T-stress is compressive whereas directionally unstable when the T-stress is tensile. However, the direction of crack propagation is mostly stabilized when more than 3% mode II fracture component is present in the loading regardless of the T-stress levels in the specimens. Since the fracture sequences in adhesive bonds are closely related to the energy balance in the system, an energy balance model is developed to predict the directional stability of cracks and the results are consistent with the experimental observations. Using the finite element method, the T-stress is shown to be closely related to the specimen geometry, indicating a specimen geometry dependence of the directional stability of cracks. This prediction is verified through testing DCB specimens with various adherend and adhesives thicknesses. By testing the specimens under both quasi-static and low-speed impact conditions, and using a high-speed camera to monitor the fracture sequence, the influences of the debond rate on the locus of failure and the directional stability of cracks are investigated. Post-failure analyses suggest that the failure tends to be more interfacial when the debond rate is low and tends to be more cohesive when the debond rate is high. However, this rate dependence of the locus of failure is greatly reduced when more advanced surface preparation techniques are used in preparing the specimens. The post-failure analyses also reveal that cracks tend to be more directionally unstable as the debond rate increases. Finally, employing interface mechanics and extending the criteria for the direction of crack propagation to adhesively bonded joints, the crack trajectories for directionally unstable cracks are predicted and the results are consistent with the overall features of the crack paths observed experimentally.

ACKNOWLEDGEMENTS

The author wishes to thank the following people without whom this work would not be possible.

- Dr. David A. Dillard for his advice on my research and life, his encouragement, and most importantly, his patience over the last four years. The education, opportunities, and responsibilities that I have been given in the Adhesion Lab at Virginia Tech are greatly appreciated and will not be forgotten.
- Dr. John G. Dillard for his advice and help on the chemistry aspects of my research. Without Dr. Dillard's support, this dissertation would not be complete.
- All my other committee members Dr. Brian Love, Dr. John J. Lesko, Dr. Scott Case, and Dr. David Y. Gao for their suggestions and guidance. Their time and effort are greatly appreciated.
- My dearest friend Dr. Richard L. Clark, Jr. for his great support for this work. Without Dr. Clark's help, this work would take much longer.
- The National Science Foundation, Science and Technology Center for High Performance Polymeric Adhesives and Composites for the major support of this research.
- The Center for Adhesive and Sealant Science at Virginia Tech for partial support of this work.
- The Engineering Science and Mechanics Department at Virginia Tech for the use of various facilities.
- The Dow Chemical Company for supplying the raw materials.
- Dr. Alphonsus from 3M Company for helpful discussions.
- Bob Simonds and Shu Guo from Engineering Science and Mechanics at Virginia Tech.
- Cooper Tire and Rubber Company for providing the feelings of home and supporting the final part of this dissertation. Without the understanding and warm support from Cooper, the beginning period of my employment would not be so pleasant and the deadline of completing my dissertation would not met.
- My wife and parents for their encouragement, care, sacrifice, and understanding.

TABLE OF CONTENTS

ABSTRACT	ii
ACKNOWLEDGEMENTS.....	iii
TABLE OF CONTENTS	iv
LIST OF TABLES.....	ix
LIST OF FIGURES	x

Chapter 1

INTRODUCTION	1
REFERENCES	7
FIGURES	9

Chapter 2

THE EFFECT OF THE T-STRESS ON CRACK PATH SELECTION IN ADHESIVELY BONDED JOINTS	13
ABSTRACT	13
KEYWORDS	13
INTRODUCTION.....	13
EXPERIMENTAL SECTION.....	17
Specimen Fabrication.....	17
DCB Testing	20
FRACTURE ANALYSIS	20
The T-Stress for Double Cantilever Beam Specimens.....	20
Analysis Results.....	21

TEST RESULTS AND DISCUSSION	22
T-Stress and Directional Stability of Cracks	22
The Effect of Adherend Bending on the Directional Stability of Cracks	23
SUMMARY AND CONCLUSIONS	24
ACKNOWLEDGMENTS	26
REFERENCES	27
FIGURES	30

Chapter 3

NUMERICAL ANALYSIS OF DIRECTIONALLY UNSTABLE CRACK PROPAGATION IN ADHESIVELY BONDED JOINTS	45
ABSTRACT	45
KEYWORDS	45
INTRODUCTION	45
ENERGY BALANCE AND DIRECTIONAL STABILITY OF CRACK PROPAGATION.....	49
INTERFACE MECHANICS AND THE PREDICTION OF CRACK TRAJECTORIES.....	54
SUMMARY AND CONCLUSIONS	58
ACKNOWLEDGMENTS	59
REFERENCES	60
FIGURES	62

Chapter 4

CRACK PATH SELECTION IN ADHESIVELY BONDED JOINTS: THE ROLES OF EXTERNAL LOADS AND SPECIMEN GEOMETRY.....	76
ABSTRACT	76
KEYWORDS	76

INTRODUCTION.....	77
EXPERIMENTAL SECTION.....	80
Specimen Fabrication.....	80
Testing and Post-Failure Analysis Methods.....	82
Quasi-static DCB test (Symmetric and Asymmetric).....	82
Low-speed impact DCB test.....	82
End notch flex (ENF) test.....	83
X-ray photoelectron spectroscopy (XPS).....	83
Scanning electron microscopy (SEM).....	84
Auger electron spectroscopic depth profile.....	84
FRACTURE ANALYSIS.....	84
The Fracture Mode Mixity in Asymmetric DCB Tests.....	84
Analysis Results.....	86
TEST RESULTS AND DISCUSSION.....	86
Fracture Mode Mixity and the Locus of Failure.....	86
Fracture Mode Mixity and the Directional Stability of Cracks.....	88
Rate of Debonding and the Locus of Failure.....	89
Rate of Debonding and the Directional Stability of Cracks.....	90
Adhesive Thickness and the Directional Stability of Cracks.....	91
CONCLUSIONS AND COMMENTS.....	92
ACKNOWLEDGMENTS.....	93
REFERENCES.....	94
TABLES.....	97
FIGURES.....	100

Chapter 5

CRACK PATH SELECTION IN ADHESIVELY BONDED JOINTS: THE ROLE OF MATERIAL PROPERTIES	113
ABSTRACT	113
KEYWORDS	114
INTRODUCTION.....	114
FRACTURE ANALYSIS	118
A Parametric Study of the Directionally Unstable Crack Propagation.....	118
Analysis Results	119
MATERIALS AND EXPERIMENTS	120
TEST RESULTS AND DISCUSSION	122
Surface Preparation and Mixed Mode Fracture Tests	122
Surface Preparation and the Rate Dependence of the Locus of Failure	124
Asymmetric Surface Preparation and the Directionally Unstable Cracks	126
Toughness of the Adhesive and the Directional Stability of Cracks	126
CONCLUSIONS AND COMMENTS	127
ACKNOWLEDGMENTS	128
REFERENCES	129
TABLES	131
FIGURES	136

Chapter 6

FUTURE WORK.....	145
INTRODUCTION.....	145
FUNDAMENTAL PHYSICS FOR THE RATE DEPENDENCE OF LOCUS OF FAILURE	146

INTERACTIONS OF MULTIPLE CRACKS	147
Vita	148

LIST OF TABLES

Chapter 4

Table. 1.	The XPS elemental analysis results for the typical specimens selected from each test.....	97
Table. 2.	Auger depth profile results for the typical specimens selected from each test.....	98
Table. 3.	The XPS elemental analysis results on both fast and slow regions of a typical DCB specimen tested quasi-statically.	99

Chapter 5

Table. 1.	Material characterization results of the epoxy adhesive formulations used in the study.	131
Table. 2.	The XPS elemental analysis results for typical specimens selected from each test. The adherends of the specimens were prepared using an acetone wipe, a base/acid etch, or a P2 etch.....	132
Table. 3.	The Auger depth profile results for typical specimens selected from each test. The adherends of the specimens were prepared using an acetone wipe, a base/acid etch, or a P2 etch.....	133
Table. 4.	The XPS elemental analysis results of the symmetric DCB specimens with either an acetone wipe or a P2 etch surface preparation.....	134
Table. 5.	The XPS elemental analysis results on the failure surfaces of the DCB specimen with asymmetric surface preparation.	135

LIST OF FIGURES

Chapter 1

- Fig. 1.** Different locus of failure and crack trajectories observed in mode I testing of adhesively bonded double cantilever beam (DCB) specimens. 9
- Fig. 2.** A crack under pure shear loading. The direction of crack propagation is perpendicular to the direction of maximum tension. 10
- Fig. 3.** The direction of crack propagation can be determined by maximizing the strain energy release rate as a function as the crack kinking angle. 11
- Fig. 4.** For a crack under mixed mode loading, the crack will propagate along a trajectory such that mode I fracture is maintained at the crack tip. 12

Chapter 2

- Fig. 1.** Different locus of failure and crack trajectories observed in mode I testing of adhesively bonded double cantilever beam (DCB) specimens. 30
- Fig. 2.** A crack in an adhesive bond, the model used in the analysis by Fleck, Hutchinson, and Suo [1] and Akisanya and Fleck [4, 16]. The adherend is assumed to be semi-infinite and the bond is under a mixed mode far field loading. 31
- Fig. 3.** Geometry of adhesively bonded double cantilever beam (DCB) specimens. 32
- Fig. 4.** Schematic of DCB specimens loaded in tension in a universal test machine until the adherends were plastically deformed in order to alter the residual stress state in the adhesive layer. 33
- Fig. 5.** The stress-strain curve for the DCB specimens under uniaxial tension and neat adhesive dogbone specimens. 34
- Fig. 6.** The numerical DCB model used in the finite element analysis; a layer of adhesive is sandwiched between two adherends. Both adhesive and adherend are modeled as linear elastic materials with material constants $E_1 = 70$ GPa, $E_2 = 2.97$ GPa, and $\nu_1 = \nu_2 = 0.33$ 35

Fig. 7.	The finite element mesh around the crack-tip. Eight nodes, plane-strain elements were used with reduced integration and quarter point singular elements were constructed around the crack tip.	36
Fig. 8.	The T-stresses for DCB specimens with different adherend thicknesses and zero residual stress.	37
Fig. 9.	The specimen geometry dependence of the T-stress in DCB specimens for specimens with no residual stress. Solid line represents Fleck, Hutchinson, and Suo [1] solution for semi-infinite adherends.	38
Fig. 10.	The observed fracture surfaces in DCB specimens with different levels of plastic deformation. From left to right, the failures are cohesive with directionally stable crack, cohesive with oscillatory crack trajectory, and interfacial (or very close to the interface) with alternating crack trajectory.	39
Fig. 11.	Details of the failure surfaces of the DCB specimen with $T = 29$ MPa, in which oscillatory crack propagation was observed. The adhesive thickness of the specimen is 0.5 mm.	40
Fig. 12.	Details of the failure surfaces of the specimen with $T = 35$ MPa, in which alternating crack propagation was observed. The adhesive thickness of the specimen is 0.5 mm.	41
Fig. 13.	The cross-section of the specimen with $T = 35$ MPa and alternating crack trajectory. The picture on the right is the scanning electron microscopy (SEM) micrograph of the circled portion of the cross-section. The adhesive thickness of the specimen is 0.5 mm.	42
Fig. 14.	The measured fracture toughness of the DCB specimens with different levels of plastic deformation. Error bars represent ± 1 standard deviation.	43
Fig. 15.	The effect of adherend thickness on the T-stress level and the directional stability of cracks. The crack tends to be more directionally unstable when the thickness of adherend decreases.	44

Chapter 3

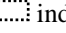

Fig. 1.	A crack within the adhesive layer in an adhesive bond. The adherend is designated as material 1 and adhesive is designated as material 2. The coordinate system is set at the crack tip.....	62
Fig. 2.	The cross-section of the failed specimen with $T = 35$ MPa and alternating crack trajectory. The picture on the right is the scanning electron microscopy (SEM) micrograph of the circled portion of the cross-section.....	63
Fig. 3.	The idealized crack trajectory geometry used in references 1 and 2.....	64
Fig. 4.	A double cantilever beam (DCB) specimen with simplified crack trajectory for directionally unstable crack propagation.....	65
Fig. 5.	The geometry and the stress state of a transverse crack in the DCB specimen with simplified crack trajectory for directionally unstable crack propagation.....	66
Fig. 6.	Available strain energy release rate for directionally unstable crack propagation in DCB specimen with various conditions.....	67
Fig. 7.	Cracks in a DCB specimen: a) interfacial crack; b) cohesive crack. The specimen is under external K_I^∞ , and K_{II}^∞ loading, which can also be described as far field stress intensity factors.....	68
Fig. 8.	The curve of local mode II stress intensity factor K_{II} versus the non-dimensional location of the sub-interfacial crack varies with the applied strain energy level.....	69
Fig. 9.	Parametric study of the local mode II stress intensity factor K_{II} versus the non-dimensional location of the sub-interfacial crack for different material combinations.....	70
Fig. 10.	The finite element mesh for predicting the crack trajectory in DCB specimen using Franc2dl.	71
Fig. 11.	Strain energy release rate (J-integral value) available at the crack tip versus the non-dimensional crack length obtained using the finite element analysis.	72
Fig. 12.	Phase angle at the crack tip versus the non-dimensional crack length obtained by the finite element analysis.....	73
Fig. 13.	Phase angle at the crack tip versus the non-dimensional interfacial crack length obtained by the finite element analysis.	74
Fig. 14.	The crack trajectory predicted by the finite element analysis using Fran2dl. The result reflects the overall characteristics of the actual crack trajectory such as the characteristic length of the crack as shown in the SEM micrograph..	75

Chapter 4

Fig. 1.	Schematic of asymmetric DCB specimens.	100
Fig. 2.	The low-speed impact test setup for DCB specimens.....	101
Fig. 3.	The geometry used in the finite element analysis to determine the fracture mode mixity in asymmetric DCB specimens. The insert is the mesh around the crack-tip.	102
Fig. 4.	The global fracture mode mixity in asymmetric DCB specimens.	103
Fig. 5.	Fracture toughnesses of the adhesive bonds measured in different tests. Error bars represent ± 1 standard deviation.....	104
Fig. 6.	Atomic force microscopy images (tapping mode) for the failure surfaces. Image a) was taken from the typical specimen tested under pure mode I, and image b) was taken from the typical specimen tested under pure mode II	105
Fig. 7.	The effect of fracture mode mixity on the directional stability of cracks in DCB specimens with high positive T-stress levels tested under low-speed impact.	106
Fig. 8.	The rate dependence of the locus of the failure in DCB specimens with negative T-stresses.....	107
Fig. 9.	The rate dependence of the locus of the failure in DCB specimens with high positive T-stresses. The T-stress in both specimens was 35 MPa.....	108
Fig. 10.	The SEM micrographs for regions with different rate of crack propagation.	109
Fig. 11.	The effect of the rate of crack propagation on the directional stability of cracks.	110
Fig. 12.	The effect of specimen geometry on the T-stress for DCB specimens.....	111
Fig. 13.	The effect of adhesive thickness on the directional stability of cracks in DCB specimens.....	112

Chapter 5

Fig. 1.	The directional stability of cracks in DCB specimens predicted using the energy balance model in reference [12]. The strain energy available is normalized to $G_C = 310 \text{ J/m}^2$	136
----------------	--	-----

Fig. 2.	The DCB specimen geometry used in the finite element analysis to determine the crack propagation behavior after the kinking occurred. The insert is the mesh around the crack-tip.....	137
Fig. 3.	The phase angle at the crack tip versus the normalized kinked crack length s/t for different materials combinations obtained from the parametric study.	138
Fig. 4.	The crack trajectories of directionally unstable crack propagation for different materials systems predicted using the finite element analysis.	139
Fig. 5.	The failure surfaces of the DCB specimens prepared using acetone wipe (a) and P2 etch (b), respectively. The  indicates the areas where XPS analyses were conducted.	140
Fig. 6.	The failure surfaces and the crack trajectory of the DCB specimen with asymmetric surface preparation. The  indicates the areas where XPS analyses were conducted.....	141
Fig. 7.	The fracture toughness of the DCB specimens using adhesives with different levels of rubber concentrations. Error bars represent ± 1 standard deviation.	142
Fig. 8.	The failure surfaces of the as-produced DCB specimens prepared using different adhesives.	143
Fig. 9.	The failure surfaces of the DCB specimens prepared using different adhesives. All the specimens contained 0.5% plastic deformation in the adherends.	144